

Induced charge signal of a glass RPC detector^{*}

HAN Ran^{1,2;1)}

¹ School of Nuclear Science and Engineering, North China Electric Power University, Beijing 102206, China

² The Institute of Nuclear physics of Lyon, Villeurbanne, 69622, France

Abstract: A gas detector glass resistivity plate chamber (GRPC) is proposed for use in the hadron calorimeter (HCAL). The read-out system is based on a semi-digital system and, therefore, the charge information from GRPC is needed. To better understand the charge that comes out from the GRPC, we started from a cosmic ray test to get the charge distribution. We then studied the induced charge distribution on the collection pad. After successfully comparing it with the prototype beam test data at CERN (European Council for Nuclear Research), the process was finally implanted into the Geant4 based simulation for future study.

Key words: glass resistivity plate chamber (GRPC), induced charge signal, beam test data, Geant4 simulation

PACS: 29.40.Cs, 29.40.Vj **DOI:** 10.1088/1674-1137/38/4/046002

1 Introduction

The International Large Detector (ILD) is a concept for a detector at the International Linear Collider (ILC). The ILC will collide electrons and positrons at energies of initially 500 GeV, upgradeable to 1 TeV [1, 2]. The ILC has an ambitious physics program, which will extend and complement that of the Large Hadron Collider (LHC). The design of the ILD is driven by these requirements. Excellent calorimetry and tracking are combined to obtain the best possible overall event reconstruction, including the capability to reconstruct individual particles within jets for particle flow calorimetry. Within the ILD paradigm of particle flow calorimetry [3], the ultimate jet energy resolution is achieved by reconstructing charged particles in the tracker, photons in the electromagnetic calorimeter (ECAL), and neutral hadrons in the ECAL and hadronic calorimeter (HCAL).

The capacity to successfully apply the particle flow algorithms can be enhanced by increasing the granularity of the different ILD sub-detectors. In the hadronic calorimeter this will doubtlessly help reduce the confusion between charged and neutral hadronic particles by providing a better separation of the associated showers. However, the cost related to such an increase in detector segmentation should be minimized. To satisfy both requirements, a gas hadronic calorimeter with a semi-digital readout is proposed (SDHCAL). The semi-digital readout will not ask the sensitive medium in HCAL to do energy measurement, so the choice of gaseous detectors offers the possibility to have very fine segmentation

while providing high detection efficiency.

2 The structure of a glass resistivity plate chamber (GRPC)

The GRPC is one of the gaseous detectors that has been proposed for use in the ILD because it can be built in large quantities at low cost. Large GRPCs, such as those required for the ILD HCAL, can be easily produced [4]. This is an important advantage with respect to other detectors (bakelite RPC also) since it guarantees very good homogeneity. However, the GRPCs for use in the ILD HCAL need to be more elaborate. Since the HCAL is situated inside the magnet coil, the sensitive medium thickness is an important issue. Very thin GRPCs are requested and 3.0 mm thick GRPCs were indeed produced and successfully tested. In Fig. 1 a scheme of such a single gap GRPC is shown. Precision ceramic balls of diameter 1.2 mm are used as spacers to separate the glass electrodes of thickness 0.7 mm (anode) and 1.1 mm (cathode). The gas volume is closed by a glass fibre frame. Read-out pads of area 1 cm by 1 cm are isolated from the anode glass by a thin Mylar foil. These pads are etched on one side of a PCB, and on the other side are located the front-end read-out chips. Finally, a polycarbonate spacer ('PCB support' in Fig. 1) is used to 'fill the gaps' between the read-out chips and to improve the overall rigidity of the detector's electronics 'sandwich'. The total theoretical thickness of the assembly is 5.825 mm.

Received 4 June 2013

^{*} Supported by Fundamental Research Funds for the Central Universities Southwest University for Nationalities (JB2012092)

1) E-mail: han.ran@gmail.com

©2014 Chinese Physical Society and the Institute of High Energy Physics of the Chinese Academy of Sciences and the Institute of Modern Physics of the Chinese Academy of Sciences and IOP Publishing Ltd

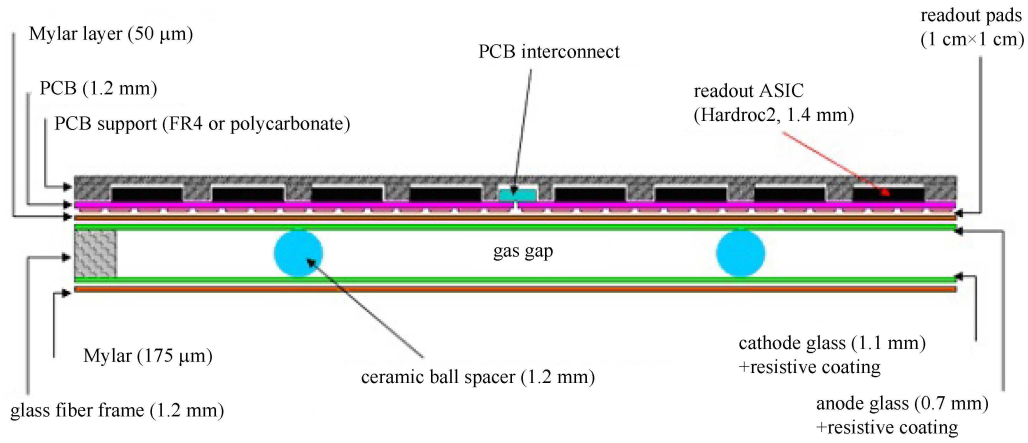


Fig. 1. A scheme of single gap GRPC.

To better understand the performance of a GRPC, the prototype was simulated and is validated by beam test data. In the simulated prototype we have 40 layers, in each layer there is 2 cm steel absorber. The size of each layer is 1 m×1 m, which is identical to the prototype. In addition to the absorber, each layer has one GRPC chamber that is composed of one gas gap and two glass plates, while the outer side of the glass plates was covered by a thin layer of resistive coating. A Mylar layer of 50 microns separates the anode from the pads of the electronic board, which was the same size as the GRPC; the pad is 1 cm by 1 cm, so we have in total 9216 readout channels in simulation.

3 The induced signal of the GRPC

The simulation is based on Geant4, the output from Geant4 is the deposited energy. In order to understand GRPC performance and achieve a better comparison with data, the induced charge distribution is also studied and implanted into the Geant4 package. Many papers have described the physics process of avalanche growth and induced charge [5, 6]. Here, we are using one of them to describe the induced charge distribution and to compare it with test beam data. The induced charge spectrum of RPC in avalanche mode can be described by a Polya function [7]:

$$Q = c \frac{(b+1)^{b+1}}{b!} \left(\frac{x}{a}\right)^b e^{-(b+1)\frac{x}{a}}, \quad (1)$$

$a = e^{\alpha s}$ is average multiplication factor on the gap s , b is an integer to determine the shape and c is a normalization factor. From Eq. (1), we would expect that, if the parameters are set properly, the charge distribution in simulation will be well described. In this case, we fixed these parameters by using cosmic ray test data.

3.1 The charge spectrum of a cosmic ray

The test setup is shown in Fig. 2. The detector is made of a small GRPC (32X8cm²) equipped with a 64-pad electronic board, which can be readout individually using an oscilloscope connected to a PC on which a Labview-based DAQ system was used to analysis the analog output signal. The gas mixture used to run the GRPC was made of TetraFluoroEthane (TFE, 93%), CO₂(5%) and SF₆ (2%). The high voltage applied on the GRPC was of 7.4 kV. The trigger system is made of two scintillators with an overlapping area smaller than that of the GRPC. The avalanche signal charge spectrum that was collected from few thousand events is shown in Fig. 3, together with its Polya distribution fitting curve. The parameters from Polya function p_0 , p_1 , p_2 are also shown in the Fig. 3.

To get the charge distribution on the pickup pad, two effects are included in this study: 1) impact spatial coordinates x & y ; and, 2) smearing due to resistive coating.

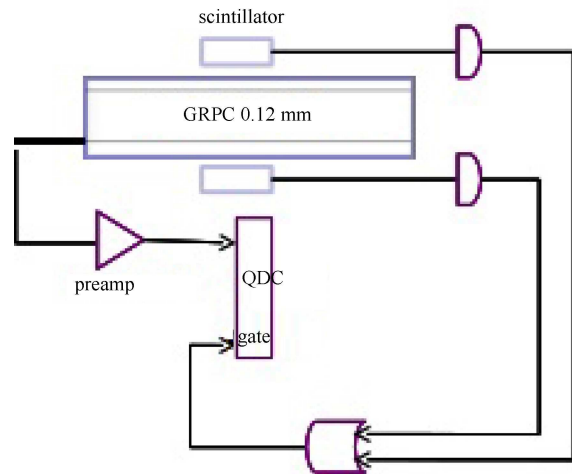


Fig. 2. (color online) Cosmic charge spectrum test setup.

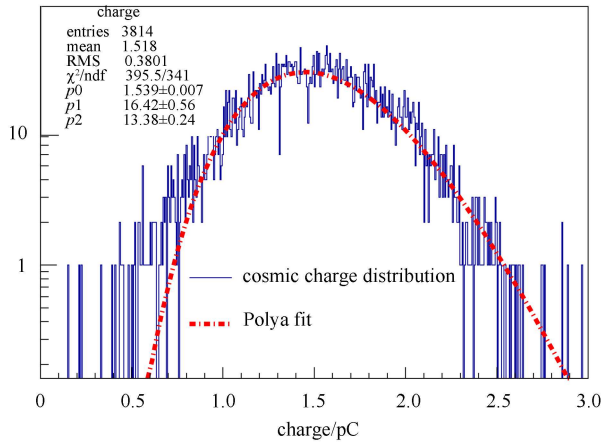


Fig. 3. Typical avalanche signal charge spectrum and its Polya fitting curve.

3.2 The induced charge distribution on a pickup pad

To calculate the induced charge distribution on the pad plane, we have considered a simplified model, as shown in Fig. 4. Here, a is the gas gap, q is the total charge getting from polya function (the charge we got after avalanche), we take it as a point charge, and d is the location of q .

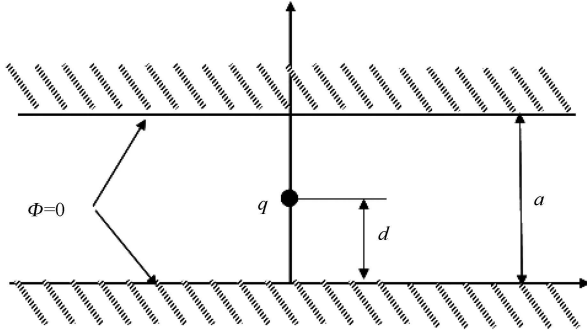


Fig. 4. Model to calculate the induced signal distribution on the pickup pad.

The potential in the gap can be expressed as in following equation [8],

$$\Phi(x, y) = 4q \sum_n \frac{1}{n} \sin\left(\frac{n\pi d}{a}\right) \sin\left(\frac{n\pi y}{a}\right) \exp\left(\mp\left(\frac{n\pi x}{a}\right)\right), \quad (2)$$

if deriving the induced charge on the surface $y=0$, then we obtain the induced charge density distribution:

$$\sigma(x) = \frac{-q}{2a} \frac{\sin\left(\frac{\pi d}{a}\right)}{\cosh\left(\frac{\pi x}{a}\right) - \cos\left(\frac{\pi d}{a}\right)}. \quad (3)$$

There is no big difference for the charge q at the gap center, bottom or top, so we take it at center, which is

$a=2d$. Then, Eq. (3) will be like

$$\sigma(x) = c \frac{-q}{2a} \frac{1}{\cosh\left(\frac{\pi x}{a}\right)}. \quad (4)$$

In Eq. (4), c is a normalized factor, which makes $\int_{-\infty}^{\infty} \sigma(x) dx = q$, $a=0.12$ cm for GRPC. The above equation corresponds to the case of $y=0$, but in our pad case this is two dimensional, so we rewrite charge density distribution

$$\sigma(x, y) = c \frac{-q}{2a} \frac{1}{\cosh\left(\frac{\pi \sqrt{(x-x_0)^2 + (y-y_0)^2}}{a}\right)}, \quad (5)$$

x_0, y_0 are the position of q , the two dimensional induced charge distribution is plotted in Fig. 5.

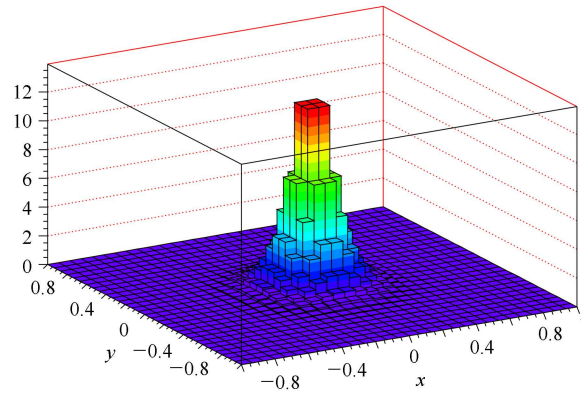


Fig. 5. The distribution of a two dimensional induced charge on the pad.

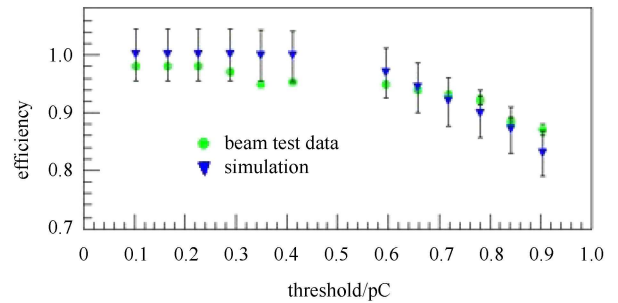


Fig. 6. (color online) Efficiency vs. threshold at $a=0.24$ cm in simulation.

3.3 Painting effect

If only the spatial effect is considered, then the cluster size of GRPC pad readout should be 1 or 2, but in reality this is not always true. One additional consideration is that the induced charge distribution is smeared with a graphite coating. Between RPC gap and the pickup pad plane there is a graphite coating layer. Depending upon the value of the resistivity of this coating layer, the

distribution of the induced charge on the pickup plane the smearing effect can be more or less large. Generally, transverse diffusion is included by distributing the charge transversally onto a disk following a Gaussian distribution with a σ increasing towards the anode ($\sigma = D_T \sqrt{l}$; where l is the drift distance) [9]. So, the smearing effect caused by the coating is a larger σ . In the simulation, this was considered as an increase in the distance of the gas gap.

4 An efficiency and multiplicity comparison with the data

We first compared the efficiency and multiplicity with

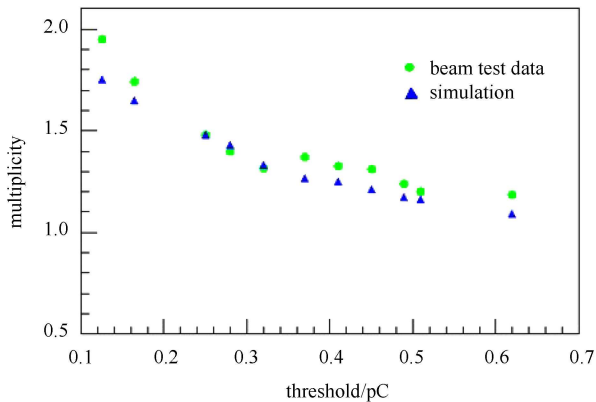


Fig. 7. (color online) Pad multiplicity vs. threshold.

the beam test at CERN 2009, where the beam is 7 GeV π^+ and the gas gap plus graphite effect leads to a gas gap of $a = 0.24$ cm. Fig. 6 shows an efficiency comparison between beam test results and simulation results, the dot points are data from a 2009 beam test at CERN, the inverted triangles are used for the simulation results. From the plot we can clearly see that, with different thresholds, the data and simulation are in good coincidence. Fig. 7 is the same but for multiplicity comparison, the dot points are data from a 2009 beam test at CERN, the triangles are used for the simulation results. These results were the first step of our comparison, we need more data to achieve a more solid conclusion about the trend.

5 Conclusion

A simulation model based on MOKKA-GEANT4 [10] package was developed with the aim of reproducing the detector response as observed in real data. The model provides an output format that is identical to the one to be used for data, so future comparison between data and simulation can be straightforward. The model will be improved by more data, which is expected from a coming Test Beam where a few units will be exposed to pion and muon beams of different energies. The Circular Electron Positron Collider is proposed to be built in China to carry out high precision study on Higgs bosons. The SDHCAL is one of the options for HCAL design. The new simulation model in this paper will be a very useful toolkit for the detector design.

References

- 1 Gateway to the Quantum Universe report - Companion document to the ILC Reference Design Report. http://www.linearcollider.org/pdf/ilc_gateway_report.pdf
- 2 Brau, James et al. Stanford Linear Accelerator Center (SLAC) SLAC-R-857, 2007
- 3 Thomson M A. Nucl. Instrum. Methods A, 2009, **611**: 25–40
- 4 Santonico R, Cardarelli R. Nucl. Instrum. Methods, 1981, **187**: 377
- 5 Christian Lippmann, Werner Riegler, Nucl. Instrum. Methods A, 2004, **517**(1): 54–76
- 6 Lippmann, Christian and Werner Riegler. Nucl. Instrum. Methods A, 2004, **533**(1): 11–15
- 7 Abbrescia M et al. Nucl. Instrum. Methods A, 1999, **431**: 413
- 8 McDonald K. Princeton physics lecture notes <http://puhep1.princeton.edu/mcdonald/examples/ph501/ph501lecture4.pdf>
- 9 Lippmann C, Riegler W, Schnizer B. Nucl. Instrum. Methods A, 2003, **508**(1): 19–22
- 10 Abramowicz H et al. EUDET-Memo-2007-17, 2007